Research Article Vol. 33, No. 19 / 22 Sep 2025 / Optics Express 39751
Optics EXPRESS

Hz-level intrinsic linewidth Brillouin fiber laser in the visible range

GEORGES PERIN,[1] EDGAR CASTA,[1] KAVYASREE ANILKUMAR,[2] PASCAL BESNARD,[1] AND STÉPHANE TREBAOL[1,*]

[1] Univ Rennes, CNRS, Institut FOTON - UMR 6082, F-22305 Lannion, France
[2] Institute of Photonics and Quantum Sciences (IPaQS), Heriot-Watt University, Edinburgh, UK
[*] stephane.trebaol@enssat.fr

Abstract: We report on the development and characterization of a compact visible Brillouin fiber laser. The laser is designed in a short cavity configuration and demonstrates an output power of 30 mW. Detailed analysis reveals an intrinsic linewidth of 6 Hz, indicating exceptional spectral purity. Comprehensive gain characterization was performed as a function of pump power, providing critical insight into the laser's performance and limitations. These findings contribute to the advancement of compact, highly stable visible fiber lasers for quantum technologies and microwave photonics.

1. Introduction

There is an increasing demand for narrow linewidth, high-power lasers in the visible spectrum, especially for atomic physics applications, such as atomic clocks [1], quantum sensing [2], quantum computing [3] or quantum gas microscopy [4–6].

Currently, most solutions involve nonlinear frequency conversion of narrow linewidth infrared lasers [7]. While these methods provide state-of-the-art performance, they typically require multiple stages.

An alternative approach is to use Stimulated Brillouin Scattering (SBS) to develop lasers that could combine narrow linewidth with high output power. First SBS demonstrations in fibers were reported in the early 80's in the visible range at 515 nm and 632 nm mainly due to the availability of high-power pump lasers [8,9]. Brillouin laser proofs of concept have been reported in hybrid and long cavity configurations [10], but due to the lack of stability and high optical losses, the reported laser performances were limited. Thanks to the development of low loss fibers and efficient fiber components for telecom applications in the C- and O-band, Brillouin fiber lasers have been reported at 1.55 µm [11,12]. Thus, fiber-cavity based Brillouin lasers have shown their ability to achieve very narrow linewidths in the sub-kHz range [12–17] and recently even in the mHz range [18,19]. Such SBS Brillouin fiber lasers have been demonstrated in other wavelength ranges, such as the neodymium (~9xx nm) [20], the ytterbium range (~10xx nm) [16], and the thulium (~18xx nm) [21] but those in the visible range are lacking.

Today, the availability of more compact visible narrow pump lasers and the increasing maturity of optical fiber components, are opening up new opportunities to develop visible light SBS fiber lasers with performance comparable to that demonstrated in the telecom band. In addition, the transition from infrared to visible light also opens up new opportunities for microwave photonics. In fact, due to the larger Brillouin shift in the visible range, close to 40 GHz at 532 nm, high quality RF (Radio-Frequency) signals can be generated by heterodyning method as already demonstrated in the infrared region [22,23].

The growing demand for quantum technologies operating at visible wavelengths [4–6,24,25] has led the scientific community to optimize the performance of photonic devices, in particular

#567985 https://doi.org/10.1364/OE.567985
Journal © 2025 Received 16 May 2025; revised 13 Aug 2025; accepted 13 Aug 2025; published 11 Sep 2025

Optics EXPRESS

single-mode laser sources, fibers and integrated components [24,26–28]. The increasing maturity of these photonic building blocks now makes it possible to study SBS at visible wavelengths. Recently, only a few works have been reported: a Brillouin laser in integrated optics was reported at 674 nm [29]; SBS lasing in a free-space diamond resonator at 532 nm [30] was demonstrated; and the characterization of Brillouin gain in a microstructured fiber at 532 nm was investigated [31].

This paper reports the demonstration of a 532 nm Brillouin laser in a single-mode fiber ring cavity characterized by an intrinsic linewidth evaluated at 6 Hz and an output power of 30 mW, limited only by the available pump power. The different stages of the laser design are described in detail. In the first part, the Brillouin gain characteristics are reported, in particular the Brillouin gain value, the phonon damping rate and the evolution of the gain profile and width as a function of the pump power at 532 nm. Second, the design elements of the visible SBS laser are presented, considering more specifically single-mode emission and laser threshold, which are optimized with respect to the performance of the pump laser power and to the fiber components available at these wavelengths. Finally, the laser performance is detailed and discussed.

2. Single-mode Brillouin laser

In this work, we aim to demonstrate a low-noise, single-mode ring-cavity fiber laser emitting at 532 nm. While considering the relative performance of photonic components in this wavelength range compared to 1.55 µm, we also seek to optimize the laser threshold and the output power. To this end, we consider a doubly resonant Brillouin laser configuration for both the laser pump and the Stokes signal. The architecture is shown in Fig. 1 and called resonant pumping. The pump laser is frequency-locked to a mode of the fiber ring in order to improve the launched power in the resonance and then to reduce the lasing threshold. At sufficiently high pump power, the SBS threshold gain is reached, resulting in the generation of a counterpropagating Stokes wave. This signal is emitted at a frequency tuned from the pump frequency by the Brillouin shift, ν_B, and characterized by a full width at half maximum (FWHM) Brillouin gain, $\Delta\nu_B$. To obtain a single-mode emission, one solution is to design a short cavity such that only one cavity mode can be located below the Brillouin gain spectra. This configuration implies that the Free Spectral Range (FSR) of the cavity is larger than the Brillouin gain bandwidth in the stimulated regime (FSR>$\Delta\nu_B$) [32].

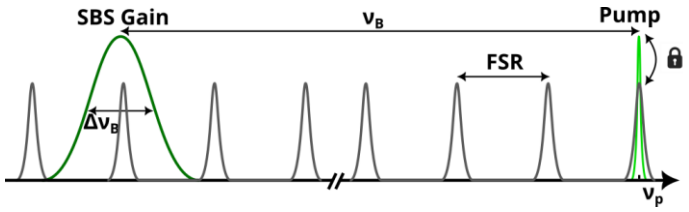

Fig. 1. Spectral arrangement of a Brillouin fiber laser in a short cavity configuration. Here the Brillouin gain linewidth is smaller than the FSR to insure single-mode operation (FSR> $\Delta\nu_B$).

At the same time, the Brillouin threshold can be lowered by increasing the effective length of the fiber ring. A longer fiber ring can increase the interaction length between the pump and the Stokes wave, thereby improving the Brillouin gain amplitude. However, this strategy introduces a trade-off in frequency selection. As the fiber ring length increases, the FSR decreases, which can lead to challenges in achieving single-mode operation and maintaining the desired resonance conditions (Fig. 1). This trade-off between lowering the threshold and effectively managing frequency selection requires careful consideration in the design of the Brillouin laser

Optics EXPRESS

system. Optimizing the fiber length while simultaneously ensuring that the laser operates in the appropriate frequency range is critical to achieving efficient laser performance. Balancing these factors will ultimately improve the overall performance of the Brillouin laser while maintaining stability in its output.

To design a visible single-mode Brillouin fiber laser, we must first know the spectral characteristics of the Brillouin gain at the target wavelength, in order to determine the dimensions of the laser cavity, in particular the maximum perimeter of the fibered cavity, so as to satisfy the single-mode emission condition while optimizing output power and low lasing threshold. The following section is dedicated to the characterization of the Brillouin gain at 532 nm, in order to provide the necessary elements for the design of the fibered cavity.

3. Brillouin gain characterization

The Brillouin gain spectral characteristics of a single-mode fiber spool (S405-XP) at 532 nm are measured as a function of pump power. Special attention is given to the identification of the transition from spontaneous to stimulated Brillouin scattering, which allows to determine critical parameters for Brillouin laser design, namely the Brillouin gain g_B, the phonon damping rate $\Gamma/2\pi$, and the gain linewidth variation $\Delta\nu_B$ in function of the input pump power. The experimental setup for the Brillouin gain characterization is shown in Fig. 2. The pump laser is a 20 kHz narrow linewidth single-mode DPSS (Diode Pump Solid State from Oxxius) emitting at 532 nm with a linear polarization state delivering 300 mW. The laser free-space output is sent through a half-wave plate and a polarization beam splitter (PBS), acting as a variable optical attenuator, to control the input pump power used for gain characterization (P_{in}). Using a 50/50 beam splitter (BS), half of this power is launched into a 1 km fiber spool with a coupling efficiency of 65%, the other part being used to monitor the input pump power. By measuring a propagation loss of 10 dB/km, it can be determined that a 1 km spool of fiber provides an effective length, L_{eff} of 390 m by using [33]:

$$L_{eff} = \frac{1 - \exp(-\alpha L)}{\alpha} \tag{1}$$

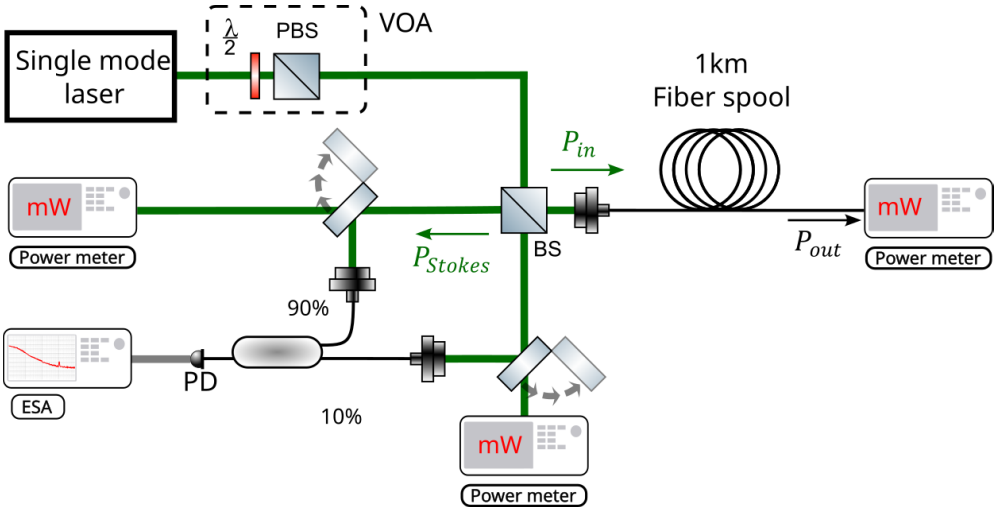

Fig. 2. Schematic of the experimental setup used to characterize the Brillouin gain inside a 1 km S-405XP fiber spool. VOA-Variable optical attenuator, PBS-Polarization beam splitter, BS-Beam splitter, PD-Photodetector.

Optics EXPRESS

With α, the propagation losses expressed in m^{-1}. The backscattered Stokes power (P_{Stokes}) is then collected by the 50/50 beam splitter. The Stokes signal is either sent to a power meter, or to a 90/10 coupler, where it is mixed with part of the pump on a fast photodetector (Thorlabs BP-40 GHz bandwidth). The resulting beat signal allows the characterization of the Brillouin gain profile on a 50 GHz electrical spectrum analyzer (ESA, Anritsu MS2668C). This heterodyne technique is a highly effective way to overcome the resolution limitations commonly faced in optical spectrum measurements [29,33], especially when dealing with closely spaced signals such as the pump and Brillouin wavelengths.

Figure 3 shows Brillouin gain spectra for input powers (P_{in}) of 10 mW (Fig. 3(a)) and 50 mW (Fig. 3(b)). From these measurements, a Brillouin shift of $\nu_B = 32.84\ GHz$ is obtained, which is very close to 32.75 GHz calculated using [34]:

$$\nu_B = \frac{2N\ V_a}{\lambda_P} \tag{2}$$

with N the effective index, V_a the acoustic velocity in the fiber and λ_P the pump wavelength. The S-405XP has a pure silica core with an effective index $N = 1.462$ and an acoustic velocity of $V_a = 5960\ m/s$ [34].

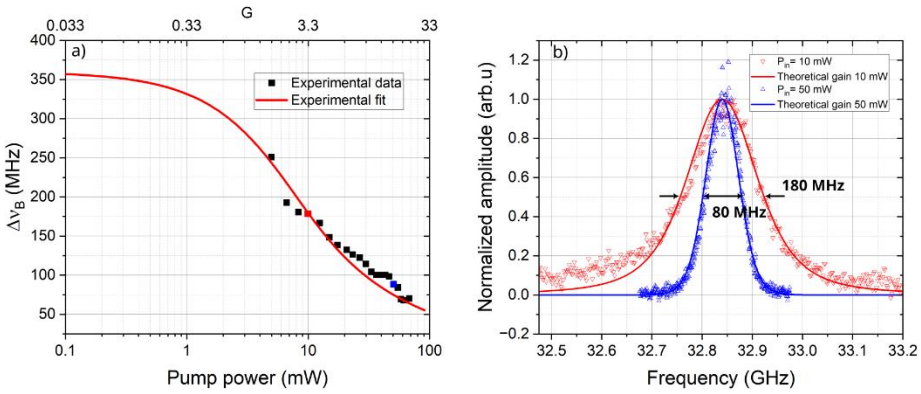

Fig. 3. a) Characterization of the Brillouin gain linewidth versus the input pump power in a 1 km S405XP single-mode fiber. Fitting curves are produced from Eq. (3). The red and blue dots correspond to spectra of Fig. b). b) Comparison of the Brillouin gain spectra resulting from the beat between the Stokes and pump signals far from the threshold ($P_{in} = 10\ mW$, red triangles) and close to the threshold ($P_{in} = 50\ mW$, blue triangles), the measurement was done with a resolution bandwidth of 1 MHz. The red and blue curve correspond to a simulation of the gain shape based on Eq. (3) for P_{in} =10 and 50 mW respectively.

The Brillouin gain linewidth $\Delta\nu_B$, is extracted for pump powers varying from 5 to 70 mW (Fig. 3(a)). A significant narrowing of the linewidth of the Stokes back-scattered signal is observed, from 250 MHz to 75 MHz when increasing the input pump power. This spectral narrowing is accompanying the transition from spontaneous to stimulated Brillouin scattering [35–37]. Consequently, the Brillouin gain spectrum can be model using [37]:

$$S(\nu) = \frac{8\pi\hbar\nu_s(\bar{n}+1)}{NcA_{eff}\Gamma}\left[exp\left[\frac{G\left(\frac{\Gamma}{4\pi}\right)^2}{\nu^2+\left(\frac{\Gamma}{4\pi}\right)^2}\right]-1\right] \tag{3}$$

With ν_s the Stokes frequency, A_{eff} the effective area, $\bar{n}$ the mean number of phonons per mode of the acoustic field, Γ the phonon decays rate and $G = \frac{g_B P_{in}}{A_{eff} K} * L_{eff}$ the single pass gain where K is the polarization factor, estimated to 3/2 in single-mode fibers [34].

Optics EXPRESS

Subsequently, measured Brillouin gain spectra are fitted using Eq. (3) from which, the Brillouin gain is estimated to $g_B = 1.62 \pm 0.17 * 10^{-11}\ m.W^{-1}$. The phonon decay rate can also be deduced from this fitting procedure to $\Gamma/2\ \pi = 360$ MHz, following the expression [37]:

$$\Gamma = \frac{2\pi N_{eff}^7 p_{12}^2}{c\lambda^2 \rho V_a g_B} \tag{4}$$

With p_{12} the photo-elastic constant and ρ the material density. Parameter values are reported in Table 1. The SBS threshold is evaluated to 70 mW, considering that this operating regime is reached when the backscattered Stokes power equals 1% of the input pump power P_{in} [38].This SBS threshold corresponds to a single pass gain $G_{th} = 21$, which is commonly reported in the literature for such single-mode fibers [38–44].

Table 1. Values of the different parameters used to fit the value of g_B

Parameters		Value
Photo-elastic constant [34]	p_{12}	2210
Density [34]	ρ (kg/m^3)	0.271
Acoustic velocity [34]	V_a (m/s)	5960
Effective area (S405 XP)	A_{eff} (μm^2)	13.9±1.8

Figure 3(b) display the fitted gain spectra for $P_{in} = 10$ mW (red curve) and $P_{in} = 50$ mW (blue curve). The experimental and theoretical curves are well superimposed and display an evolution from a Lorentzian shape as expected for the spontaneous regime, to a Gaussian shape, for G≫1 as suggested by Eq. (3).

4. Cold cavity

The cold cavity design is a fundamental aspect of Brillouin laser operation, because it determines the resonant properties of the cavity, including the FSR and the Q-factor. These parameters directly influence the interaction between the pump light and the medium, which is essential for efficient Stokes wave generation [45].

As discussed in section 1, a simple approach to realize a single-mode BFL is to use a cavity with an FSR, higher than the stimulated Brillouin gain linewidth, $\Delta\nu_B = 75$ MHz. Considering, the characterization of the SBS linewidth from the previous section, a 1.4 m fiber ring implies an FSR $= c/NL = 158$ MHz, ensuring the single-mode operation of the laser at 532 nm. The fiber ring is made using a commercial Thorlabs coupler made from S460-HP showing similar properties than the S405-XP fiber used for Brillouin gain characterization.

The experimental setup for the fiber Brillouin laser characterization is shown in Fig. 4.

The pump laser is similar to the one used in the Brillouin characterization setup (Fig. 2). To overcome the lack of laser wavelength tunability, a portion of the fiber cavity is coiled around a cylindrical piezoelectric (PZT) cell, which allows the fiber to be stretched by applying a voltage, thereby allowing frequency tuning of the cavity mode resonances over 600 MHz at a rate of 8 MHz/V.

The cavity was characterized by sending a low input pump power to avoid the excitation of nonlinearities such as thermal and Brillouin effects. The normalized experimental transfer function is shown by the black curve in Fig. 5. The theoretical function (red dashed curve) is superimposed.

The two curves are superimposed, validating the value of the parameters used for the simulation and allowing us to extract a value of κ of 73%. The free spectral range of the cavity is FSR $= 158$ MHz, and the resonance linewidth $\Delta\nu = 10$ MHz gives a quality factor of 5.6×10^7.

Optics EXPRESS

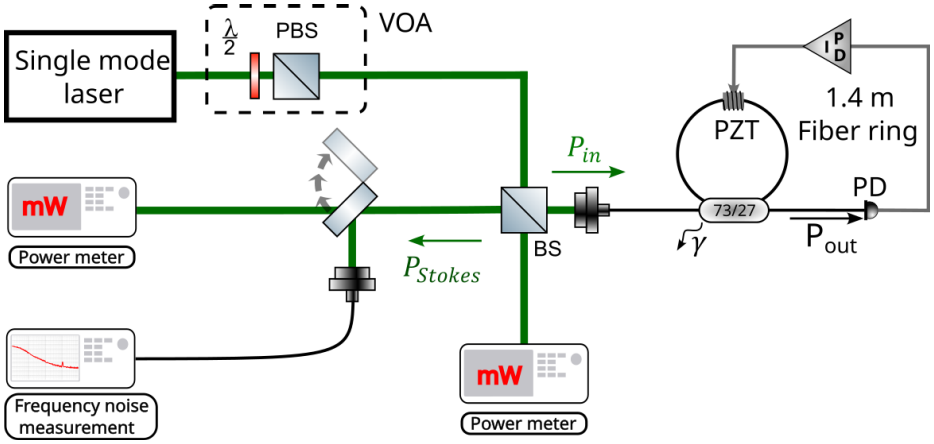

Fig. 4. Schematic of the experimental setup for the realization of a fiber Brillouin laser. The PZT allows the cavity resonance to be tuned over 600 MHz. When using side-lock optoelectronic feedback loop, the pump laser is kept in resonance with a cavity mode. The Stokes power is either sent to the power meter or to a frequency noise measurement setup.

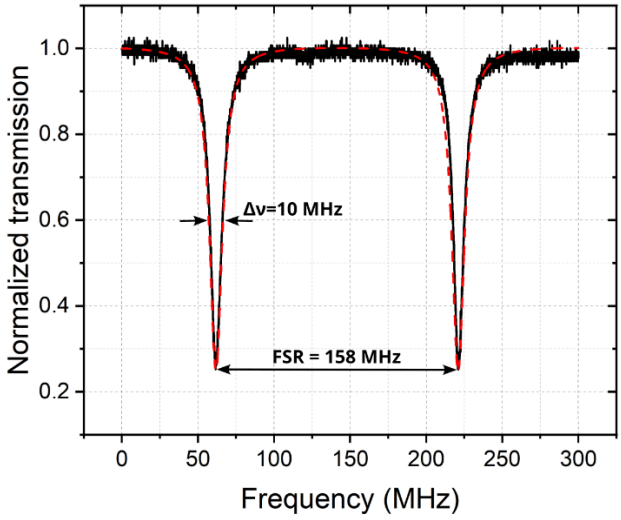

Fig. 5. Comparison between the experimental transmission of a 1.4 m fiber ring made by using a 70/30 coupler (black curve) and the cavity transmission (red dash curve) [46].

5. Brillouin laser

5.1. Static characterization

To operate the Brillouin laser in the resonant configuration described in section 1, it is essential to keep the pump wavelength in resonance with a mode of the fiber ring (Fig. 1). Thus, the input pump power efficiently drives the stimulated Brillouin scattering and generates a lasing SBS signal. To implement the side-locking scheme shown in Fig. 4, the transmitted pump signal (P_{out}) is used to lock the cavity mode onto the laser frequency. The cavity output is compared to a signal at half the resonance transmission level (Fig. 5), and the electronic error signal is then fed to a PID (Proportional, Integral, Derivative) controller, which applies a correction voltage to

Optics EXPRESS

the cylindrical PZT. As we are using a PZT component, the correction bandwidth is limited to around 10 kHz.

Thanks to a flip mirror, the laser SBS signal is fed back to either a power meter or a frequency noise (FN) measurement scheme to assess the stability and performance of the laser.

The L-L curve of the visible Brillouin laser (Fig. 6(a)) is characterized by a lasing threshold of 26 mW and a slope efficiency of 83%. To compare threshold and slope efficiency values with theoretical ones, we used a model based on the work of Toyama *et al.* [47]. The first Stokes threshold is given by:

$$P_{thS1} = P_{th}\frac{\left(1-\sqrt{\kappa\kappa_r}\right)^2}{(1-\kappa)(1-\gamma)} \tag{5}$$

Where the threshold power inside the cavity is P_{th} and the cavity round-trip loss is $\kappa_r = (1-\gamma)(1-s)e^{-\alpha L}$ with γ is coupler losses, s is the splicing losses and α is the fiber propagation losses. The slope of the Brillouin L-L curve is derived from:

$$S = \frac{((1-\gamma)(1-\kappa))^2}{\left(1-\sqrt{\kappa\kappa_r}\right)^2\left(\left(1+\sqrt{\kappa\kappa_r}\right)^2-1\right)} \tag{6}$$

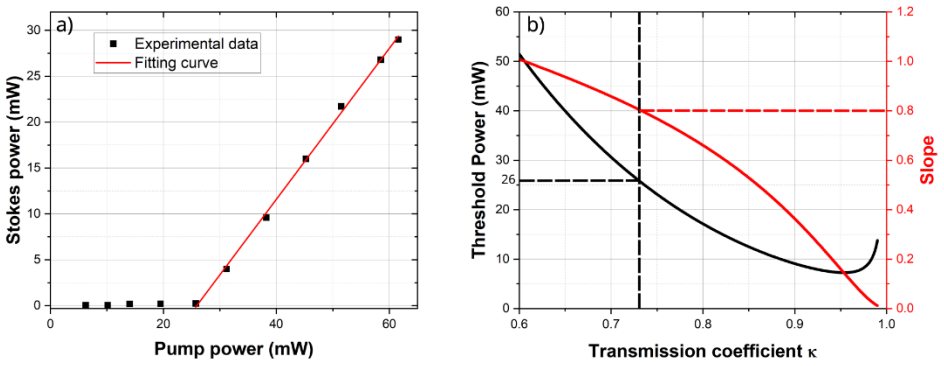

Fig. 6. a) Stokes power of the 1.4 m Brillouin fiber laser vs pump power (L-L curve) with a threshold of 26 mW and a slope of 83% (black points) as determined by a linear fit of the data points above the threshold (red curve). b) Simulation of the threshold and the slope of the Brillouin laser again the variation of the transmission coefficient κ. The values of the parameters used in the simulation are given in Table 2.

Table 2. Values of the different parameters used to simulate the fiber ring transmission at 532 nm

Parameters		Values
Cavity perimeter	L (m)	1.4
Coupler loss	γ (dB)	0.3
Fiber propagation loss	α (dB/km)	10
Splicing loss	s (dB)	0.1
Round-trip transmission	κ_R	0.88

Figure 6(b) shows the theoretical Stokes threshold P_{thS1} and the slope S as a function of the coupling parameter κ. For a measured coupling coefficient of 73%, simulated threshold is 26 mW and slope efficiency is 80%, both values are in good agreement with the experimental data. We

Optics EXPRESS

can also see in Fig. 6(b) that for a higher value of κ, the threshold can be lowered but at the cost of a laser slope decreasing. This trade-off is important to keep in mind when designing future cavity in order to be able to obtain a Brillouin laser with maximum output power in the resonant pump regime.

Moreover, due to the lack of any suitable amplifier in the visible range, the maximum output power of the Brillouin laser is also determined by the available pump power (62 mW in the current configuration) and the cavity design. The maximum reachable Stokes power can be calculated using Eqs. (5) and (6). It is possible to estimate that the maximum power achievable with the current design is around 30 mW, which is close to the value of 29 mW that we obtain with our setup. Without any pump limitation, the maximum Stokes power achievable in the current configuration is 46 mW for a pump power of 82 mW.

5.2. *Frequency noise characterization*

Brillouin lasers are known to exhibit low-frequency noise (FN) features. In particular, the Stokes signal usually displays a narrower linewidth than the pump. To demonstrate this effect with this visible Brillouin fiber laser, a frequency noise measurement is performed with the Brillouin laser at its maximum power of 29 mW. A description of the measurement setup is given in the following Refs [27,48,49]. and is detailed in the Supplement 1. This setup allows the measurement of frequency noise from 100 to 100 kHz with a noise floor of 0.1 Hz^2/Hz. The Brillouin laser's RIN is approximately -130 dBc/Hz over the measurement bandwidth. It is the primary cause of the noise floor. The FN measurement of the pump laser and the one of the Brillouin fiber laser are shown in Fig. 7.

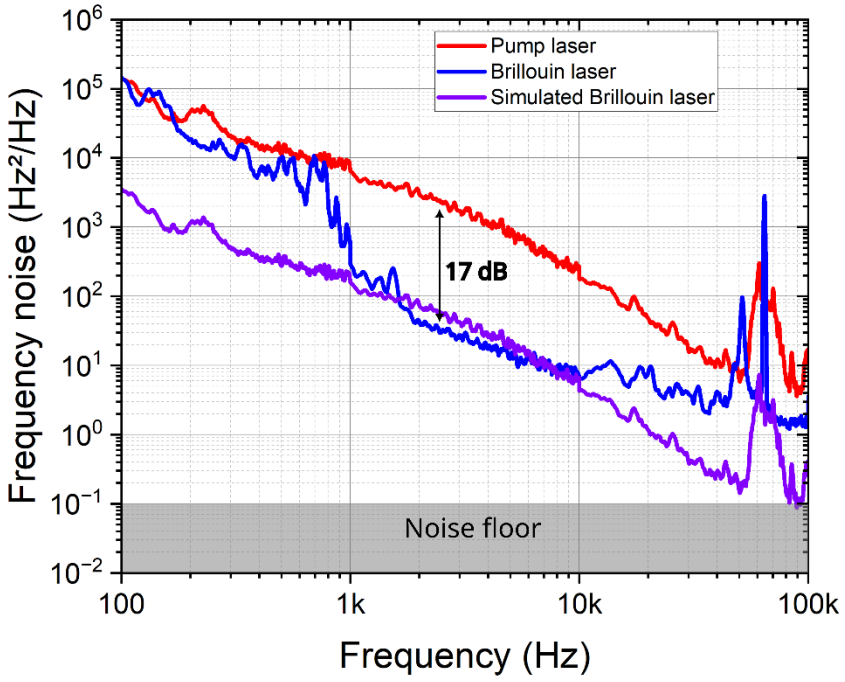

Fig. 7. Comparison of the pump laser (red curve), Brillouin fiber laser (blue curve) and simulated Brillouin laser (purple curve) frequency noises. The origin of the peaks observed around 60 kHz should probably be attributed to the intensity noise of the pump laser.

The frequency noise of the pump laser exhibits a classical shape with a $1/f^2$ slope, and reaches a white frequency noise of 4 Hz^2/Hz giving an intrinsic linewidth of 12 Hz. The integrated

Optics EXPRESS

linewidth is determined using the Elliot formula [50] and give a value of 12 kHz at 10 ms (similar estimation is obtained using the betaline approach [51]). The origin of the spike around 60 kHz should probably be attributed to the intensity noise of the pump laser.

The frequency noise of the Brillouin laser shows a reduction of up to 17 dB compared to the pump laser between 1 kHz and 10 kHz, reaching a white frequency noise of 2 Hz^2/Hz above 70 kHz, which corresponds to an estimated intrinsic linewidth of 6 Hz. This measured linewidth is two orders of magnitude smaller than previously reported work in the visible range [29]. For frequencies below 1 kHz, the SBS laser noise increases to the level of the pump laser, which leads to an integrated linewidth at 10 ms of 8 kHz, close to the pump laser integrated linewidth.

SBS laser FN can be divided in three contributions namely the transferred pump laser noise, technical noises, and a fundamental noise related to spontaneous Brillouin scattering. The principal contribution is usually the phase noise of the pump laser, which is transmitted to the SBS laser after being attenuated [35]. This first contribution can be modeled as follows:

$$S_B(f) = -\frac{\ln(\kappa\kappa_r)}{\left(\frac{2\pi\Delta\nu_B}{FSR}\right) - \ln(\kappa\kappa_r) + 2i\pi f\tau} \times \frac{e^{-\pi f\tau}\sin(\pi f\tau)}{\pi f\tau} S_{pump}(f) \tag{7}$$

Where $S_B(f)$ is the frequency noise of the Brillouin laser, $S_{pump}(f)$ is the frequency noise of the pump laser, $\tau = \frac{nL}{c}$ is the fiber ring roundtrip time and $\Delta\nu_B$ is the Brillouin gain linewidth in the stimulated regime.

The simulated FN (purple curve) is displayed in Fig. 7, by using experimentally determined parameters. We can see that between 1 kHz and 10 kHz the experimental and simulated FN are in good agreement.

Below 1 kHz, the SBS laser noise increase can be attributed to the pump technical noise transferred on the Brillouin cavity FN through the 1 kHz bandwidth optoelectronic locking. Above 10 kHz, the simulated FN noise suggests that SBS laser FN could reach the 10^{-1} Hz^2/Hz regime that would correspond to a 100 mHz intrinsic linewidth.

Improving the sensitivity of the frequency noise measurement bench, the optoelectronic servo-control and the thermal and mechanical packaging of the laser cavity should enable to achieve such performances in future.

Finally, the fundamental white noise contribution to the SBS laser FN related to the spontaneous Brillouin scattering can be estimated [52] to 0.017 Hz^2/Hz (50 mHz intrinsic linewidth), well below the measured SBS laser FN.

6. Conclusion

We report a narrow linewidth Brillouin fiber laser at 532 nm characterized by an intrinsic linewidth of 6 Hz, a threshold of 26 mW and a pump-limited output power of 29 mW. The design of this single-mode laser is based on an in-depth study of the Brillouin gain as a function of the pump power. It shows the shift from the spontaneous Brillouin scattering regime to the stimulated Brillouin scattering regime characterized by a 75 MHz linewidth. The continuous improvement of fibered photonic components at visible wavelengths should allow the extension of this type of architecture to shorter wavelengths, thus addressing the need for compact and low-noise lasers in the full visible spectrum.

Funding. I-DEMO PIA4 Bpifrance (40898814/1, QoQeliQo)- Région Bretagne Lannion Trégor Communauté (CPER PHOT-BREIZH); Agence Nationale de la Recherche (Fond de Relance RAINBOW).

Acknowledgement. The authors would like to thank Oxxius for providing the pump laser used for these experiments. We also thank Bramerie Laurent, Gay Mathilde and Lobo Sébastien for their technical support.

Disclosures. The authors declare no conflicts of interest.

Data availability. Data underlying the results presented in this paper are not publicly available at this time but may be obtained from the authors upon reasonable request.

Optics EXPRESS

Supplemental document. See Supplement 1 for supporting content.

References

1. Z. L. Newman, V. Maurice, C. Fredrick, *et al.*, "High-performance, compact optical standard," Opt. Lett. **46**(18), 4702–4705 (2021).
2. C. L. Degen, F. Reinhard, and P. Cappellaro, "Quantum sensing," Rev. Mod. Phys. **89**(3), 035002 (2017).
3. A. Kinos, D. Hunger, R. Kolesov, *et al.*, "Roadmap for Rare-earth Quantum Computing," arXiv (2021).
4. A. Jenkins, J. W. Lis, A. Senoo, *et al.*, "Ytterbium Nuclear-Spin Qubits in an Optical Tweezer Array," Phys. Rev. X **12**, 021027 (2022).
5. M.-D. Li, Y.-G. Zheng, W.-Y. Zhang, *et al.*, "A high-power and low-noise 532-nm continuous-wave laser for quantum gas microscopy," Rev. Sci. Instrum. **92**(8), 083202 (2021).
6. G.-B. Jo, J. Guzman, C. K. Thomas, *et al.*, "Ultracold Atoms in a Tunable Optical Kagome Lattice," Phys. Rev. Lett. **108**(4), 045305 (2012).
7. D. Darwich, R. Prakash, C. Dixneuf, *et al.*, "High power ultralow-intensity noise continuous wave laser tunable from orange to red," Opt. Express **30**(8), 12867–12877 (2022).
8. L. F. Stokes, M. Chodorow, and H. J. Shaw, "All-fiber stimulated Brillouin ring laser with submilliwatt pump threshold," Opt. Lett. **7**(10), 509–511 (1982).
9. S. P. Smith, F. Zarinetchi, and S. Ezekiel, "Narrow-linewidth stimulated Brillouin fiber laser and applications," Opt. Lett. **16**(6), 393–395 (1991).
10. D. R. Ponikvar and S. Ezekiel, "Stabilized single-frequency stimulated Brillouin fiber ring laser," Opt. Lett. **6**(8), 398–400 (1981).
11. Jihong Geng, S. Staines, Zuolan Wang, *et al.*, "Highly stable low-noise Brillouin fiber laser with ultranarrow spectral linewidth," IEEE Photonics Technol. Lett. **18**(17), 1813–1815 (2006).
12. K. H. Tow, Y. Leguillon, S. Fresnel, *et al.*, "Toward More Coherent Sources Using a Microstructured Chalcogenide Brillouin Fiber Laser," IEEE Photonics Technol. Lett. **25**(3), 238–241 (2013).
13. W. Loh, J. Becker, D. C. Cole, *et al.*, "A microrod-resonator Brillouin laser with 240 Hz absolute linewidth," New J. Phys. **18**(4), 045001 (2016).
14. Y. Qin, S. Ding, M. Zhang, *et al.*, "High-power, low-noise Brillouin laser on a silicon chip," Opt. Lett. **47**(7), 1638–1641 (2022).
15. W. Loh, S. Yegnanarayanan, F. O'Donnell, *et al.*, "Ultra-narrow linewidth Brillouin laser with nanokelvin temperature self-referencing," Optica **6**(2), 152 (2019).
16. M. Deroh, E. Lucas, K. Hammani, *et al.*, "Stabilized single-frequency sub-kHz linewidth Brillouin fiber laser cavity operating at 1 µm," Appl. Opt. **62**(30), 8109 (2023).
17. S. Gundavarapu, G. Brodnik, M. Puckett, *et al.*, "Sub-hertz fundamental linewidth photonic integrated Brillouin laser," Nat. Photonics **13**(1), 60–67 (2019).
18. A. Karuvath, A. Sebastian, and P. Besnard, "C-Band tunable Brillouin fiber-laser with sub-Hz intrinsic linewidth," in *Fiber Lasers and Glass Photonics: Materials through Applications III*, M. Ferrari, A. B. Seddon, and S. Taccheo, eds. (SPIE, 2022), Vol. PC12142, p. PC121420 V.
19. M. Alouini, G. Danion, and M. Vallet, "Self-linewidth-narrowing photonic oscillator," Opt. Express **33**(1), 1021 (2025).
20. R. Prakash, D. Darwich, C. Dixneuf, *et al.*, "Neodymium laser-pumped ultra-low noise tunable Brillouin fiber laser around 920 nm," Opt. Express **31**(25), 42495 (2023).
21. K. Hu, I. V. Kabakova, S. Lefrancois, *et al.*, "Hybrid Brillouin/thulium multiwavelength fiber laser with switchable single- and double-Brillouin-frequency spacing," Opt. Express **22**(26), 31884 (2014).
22. J. Li, H. Lee, and K. J. Vahala, "Microwave synthesizer using an on-chip Brillouin oscillator," Nat. Commun. **4**(1), 2097 (2013).
23. B. Heffernan, J. Greenberg, T. Hori, *et al.*, "Brillouin laser-driven terahertz oscillator up to 3 THz with femtosecond jitter," (2024).
24. M. Corato-Zanarella, A. Gil-Molina, X. Ji, *et al.*, "Widely tunable and narrow-linewidth chip-scale lasers from near-ultraviolet to near-infrared wavelengths," Nat. Photonics **17**(2), 157–164 (2023).
25. Z. Zhang, B. Shen, M. A. Tran, *et al.*, "Photonic integration platform for rubidium sensors and beyond," Optica **10**(6), 752 (2023).
26. T. J. Kippenberg, S. M. Spillane, and K. J. Vahala, "Demonstration of ultra-high-Q small mode volume toroid microcavities on a chip," Appl. Phys. Lett. **85**(25), 6113–6115 (2004).
27. R. Kervazo, P. Georges, A. Congar, *et al.*, "Sub-20 kHz low-frequency noise near ultraviolet butt-coupled fiber Bragg grating external cavity laser diode," Appl. Phys. Lett. **125**(16), 161102 (2024).
28. X. Lu, L. Chang, M. A. Tran, *et al.*, "Emerging integrated laser technologies in the visible and short near-infrared regimes," Nat. Photonics **18**(10), 1010–1023 (2024).
29. N. Chauhan, A. Isichenko, K. Liu, *et al.*, "Visible light photonic integrated Brillouin laser," Nat. Commun. **12**(1), 4685 (2021).
30. Z. Bai, R. J. Williams, O. Kitzler, *et al.*, "Diamond Brillouin laser in the visible," APL Photonics **5**(3), 031301 (2020).

Optics EXPRESS

31. R. I. Woodward, E. J. R. Kelleher, S. V. Popov, *et al.*, "Stimulated Brillouin scattering of visible light in small-core photonic crystal fibers," Opt. Lett. **39**(8), 2330–2333 (2014).
32. W. Loh, J. Stuart, D. Reens, *et al.*, "Operation of an optical atomic clock with a Brillouin laser subsystem," Nature **588**(7837), 244–249 (2020).
33. A. Yeniay, J.-M. Delavaux, and J. Toulouse, "Spontaneous and stimulated Brillouin scattering gain spectra in optical fibers," J. Lightwave Technol. **20**(8), 1425–1432 (2002).
34. G. Agrawal, *Nonlinear Fiber Optics and Applications on Nonlinear Fiber Optics*, 3rd Edition (2013).
35. A. L. Gaeta and R. W. Boyd, "Stochastic dynamics of stimulated Brillouin scattering in an optical fiber," Phys. Rev. A **44**(5), 3205–3209 (1991).
36. A. Villafranca, J. A. Lázaro, Í Salinas, *et al.*, "Stimulated Brillouin scattering gain profile characterization by interaction between two narrow-linewidth optical sources," Opt. Express **13**(19), 7336–7341 (2005).
37. R. W. Boyd, K. Rzaewski, and P. Narum, "Noise initiation of stimulated Brillouin scattering," Phys. Rev. A **42**(9), 5514–5521 (1990).
38. A. Kobyakov, M. Sauer, and D. Chowdhury, "Stimulated Brillouin scattering in optical fibers," Adv. Opt. Photonics **2**(1), 1 (2010).
39. K. S. Abedin, "Observation of strong stimulated Brillouin scattering in single-mode As2Se3 chalcogenide fiber," Opt. Express **13**(25), 10266 (2005).
40. R. G. Smith, "Optical Power Handling Capacity of Low Loss Optical Fibers as Determined by Stimulated Raman and Brillouin Scattering," Appl. Opt. **11**(11), 2489–2494 (1972).
41. K. Shiraki, M. Ohashi, and M. Tateda, "Performance of strain-free stimulated Brillouin scattering suppression fiber," J. Lightwave Technol. **14**(4), 549–554 (1996).
42. J. H. Lee, Z. Yusoff, W. Belardi, *et al.*, "Investigation of Brillouin effects in small-core holey optical fiber: lasing and scattering," Opt. Lett. **27**(11), 927 (2002).
43. F. Poletti, K. Furusawa, Z. Yusoff, *et al.*, "Nonlinear tapered holey fibers with high stimulated Brillouin scattering threshold and controlled dispersion," J. Opt. Soc. Am. B **24**(9), 2185–2194 (2007).
44. D. Cotter, "Stimulated Brillouin Scattering in Monomode Optical Fiber," 4, 10–19 (1983).
45. A. Sebastian, I. V. Balakireva, S. Fresnel, *et al.*, "Relative intensity noise in a multi-Stokes Brillouin laser," Opt. Express **26**(26), 33700 (2018).
46. A. Yariv, "Universal relations for coupling of optical power between microresonators and dielectric waveguides," Electron. Lett. **36**(4), 321–322 (2000).
47. K. Toyama, S. Huang, P. A. Nicati, *et al.*, "Generation of multiple Stokes waves in a Brillouin fiber ring laser," in *(Proceedings of the Ninth International Conference on Optical Fiber Sensors* 11–14 1993).
48. G. Perin, D. Mammez, A. Congar, *et al.*, "Compact fiber-ring resonator for blue external cavity diode laser stabilization," Opt. Express **29**(23), 37200 (2021).
49. O. Llopis, P. H. Merrer, H. Brahimi, *et al.*, "Phase noise measurement of a narrow linewidth CW laser using delay line approaches," Opt. Lett. **36**(14), 2713–2715 (2011).
50. D. S. Elliott, R. Roy, and S. J. Smith, "Extracavity laser band-shape and bandwidth modification," Phys. Rev. A **26**(1), 12–18 (1982).
51. G. Di Domenico, S. Schilt, and P. Thomann, "Simple approach to the relation between laser frequency noise and laser line shape," Appl. Opt. **49**(25), 4801 (2010).
52. J. Li, H. Lee, T. Chen, *et al.*, "Characterization of a high coherence, Brillouin microcavity laser on silicon," Opt. Express **20**(18), 20170 (2012).